Design and analysis of a series-parallel hybrid 3-SPS-U mechanism

Swaminath Venkateswaran, Damien Chablat, Denis Creusot

Proceedings of the ASME 2023
International Design Engineering Technical Conferences & Computers and Information in Engineering Conference
IDETC/CIE 2023
August 20–23, 2023, Boston, MA

DETC2023-115225

DESIGN AND ANALYSIS OF A SERIES-PARALLEL HYBRID 3-SPS-U MECHANISM

Swaminath Venkateswaran [1,†,*], Damien Chablat [2,†], Denis Creusot [2]

[1]Léonard de Vinci Pôle Universitaire, Research Center, 92916 Paris La Défense, France
[2]Centre National de la Recherche Scientifique (CNRS), Laboratoire des Sciences du Numérique de, Nantes (LS2N), UMR CNRS 6004, 44321 Nantes, France

ABSTRACT

This article presents the design and analysis of a series-parallel hybrid mechanism. The mechanism has two stages which consist of a fixed base, an intermediate mobile platform and a mobile end-effector. Each stage is connected by three tension springs and a universal joint in the center. By correlating to a 3-SPS-U architecture, the geometrical equations for the mechanism are generated in the Euler space. To simplify the computations, the Tilt & Torsion space is employed for the analysis of the mechanism. A stability analysis is carried out initially to identify the optimum design parameters of the mechanism in the static mode. By employing algebraic methods, the singularity analysis of the mechanism is then carried out to generate the workspace and identify the tilt limits of the hybrid mechanism. A mapping equation which demonstrates the relation between the Tilt & Torsion angles and the Euler angles is then presented using the results of singularity analysis and numerical simulations. The mechanism under study is then proposed to be integrated on a piping inspection robot for passing through elbows and T-sections.

Keywords: Series-parallel mechanism, Tilt & Torsion, Tensegrity, Singularity analysis

1. INTRODUCTION

In many industrial applications, parallel robots also known as Parallel Kinematics Machines (PKM) are advantageous over serial robots. The main advantages of the PKM's are their lower mass/inertia properties, higher structural stiffness and better accuracy [1, 2]. At the same time, these robots have some disadvantages such as a smaller workspace when compared to their serial counterparts and poor manipulability in some regions of the workspace [3]. For overcoming these problems, hybrid mechanisms which employ two or several parallel robots in series have been developed and analyzed in recent years. These hybrid mechanisms can combine the advantages of both serial and parallel robots such as better accuracy like the parallel robot and a larger workspace like the serial robot [4]. Some latest and interesting applications of such hybrid mechanisms include: the Hybrid YamaBot 10 with 7-DOF [5], the RH5 humanoid robot [6], the cable-linkage serial-parallel palletizing robot (CSPR) [7], the bio-inspired hybrid structure of Huang et al.[8] and the hybrid 3-RPS-3-SPR robot of Nayak et al. [9]. All these recent researches have presented the advantages of combining serial and parallel architectures for addressing many engineering problems. In this article, we present a hybrid mechanism which comprises two 3-SPS-U tensegrity mechanisms stacked one over the other in series. As a part of a research project with AREVA, a rigid bio-inspired piping inspection robot was designed and developed at LS2N, France [10]. To make it flexible, a 3-SPS-U tensegrity mechanism that consists of three tension springs and a universal joint was introduced between each motor unit of the robot [11]. However, the tilt limits offered by this mechanism were around $\pm\pi/6$ radians which was significantly low [12]. To overcome this issue, we propose a stacked architecture of the tensegrity mechanism, which could potentially offer higher tilt limits when compared to the single stage parallel mechanism.

The conventional method to study the singularities for the tensegrity mechanism is carried out for the Euler angles of the universal joint as proposed in [12]. With the stacked architecture, four tilt angles must be taken into account for the analysis and this becomes complicated through the algebraic method. However, there exists an alternate approach where the modified Euler angles, more specifically known as the "Tilt & Torsion (T&T)" angles could be employed, especially when there are spherical joints [13]. The advantages of the T&T angles were proposed by Bonev et al.[14] for the study of spatial parallel mechanisms and it was also demonstrated that there exists a certain class of parallel mechanisms with zero torsion, thereby referred to as the Zero-torsion parallel mechanisms [15]. We employ these T&T angles or the modified Euler angles to analyze the hybrid 3-SPS-

[†]Joint first authors
[*]Corresponding author: swaminath.venkateswaran@devinci.fr
Documentation for `asmeconf.cls`: Version 1.34, August 28, 2023.

U tensegrity mechanism. The advantage of this approach is that it allows to analyze the entire architecture using a common azimuth angle, thereby simplifying the computations. A mapping relation is then demonstrated which permits to have a relation between the T&T space and the Euler space of the mechanism and it is validated through numerical simulations.

The outline of the article is as follows. In the following section, the architecture of the hybrid mechanism and its geometrical equations are presented in the Euler space and the T&T space. Then, we present the stability analysis of the stacked model under static modes. Followed by that, we present the singularity analysis on the mechanism and the results of workspace obtained. The subsequent section presents the mapping relation and numerical simulations of the mechanism. The article then ends with conclusions and perspectives.

2. ARCHITECTURE OF THE MECHANISM

The hybrid tensegrity mechanism under study is represented in Fig. 1a. The mechanism consists of three rigid platforms and they are interconnected through three tension springs and a universal joint in the center. In order to establish the geometric equations, each stage of the mechanism is correlated to a parallel manipulator of type 3-SPS-U [16]. Thus, we have a series-parallel hybrid 3-SPS-U mechanism and this correlation is represented in Fig. 1b. Here, S represents the spherical joint which refers to the spring mounting points, P represents the actuated prismatic joint which refers to the tension springs and U represents the universal joint. The mechanism can work under passive modes without the presence of external actuation as well as in active modes. In the active modes, the mobile platforms are actuated through cables that pass through each spring and this is accomplished with the help of three external DC-motors.

2.1 Geometrical equations in the Euler space

The hybrid mechanism represented in Fig. 1a has a total of 4 degrees of freedom with each stage having 2 degrees of freedom resulting from the Euler angles of the universal joint. In the Euler space, we use the rotation angles η, ϕ for stage-1 and the angles ζ, ψ for stage-2. These angles are represented in Fig. 1a. Also, Fig. 1 represents the home-pose of the mechanism where these tilt angles are equal to 0 radians. The fixed coordinate frame of the base is represented by $\sum_0$ and the spring mounting points are represented by $B_i (i = 1, 2, 3)$. These mounting points form an imaginary equilateral triangle of the manipulator base whose median is given by r_f. The vector coordinates for the spring mounting points of the fixed base are given by the equation:

$$\mathbf{b}_{i+1} = \left[r_f \cos\left(\frac{2\pi i}{3}\right), r_f \sin\left(\frac{2\pi i}{3}\right), -r_f h \right]^T, \quad i = 0, 1, 2 \qquad (1)$$

In Eqn. (1), h is a constant which is essential to determine the stability of the architecture under static modes. The moving coordinate frame of the intermediate mobile platform is represented by $\sum_1$ and the spring mounting points are given by $C_i (i = 1, 2, 3)$. For estimating the vector coordinates, the XY Euler angles about the axis A of the universal joint are employed. The coordinates are given by:

$$\mathbf{c}_{i+1} = \mathbf{E} \left[r_f \cos\left(\frac{2\pi i}{3}\right), r_f \sin\left(\frac{2\pi i}{3}\right), r_f h \right]^T, \quad i = 0, 1, 2 \qquad (2)$$

$$\text{where } \mathbf{E} = \begin{bmatrix} c_\phi & 0 & s_\phi \\ s_\eta s_\phi & c_\eta & -s_\eta c_\phi \\ -c_\eta s_\phi & s_\eta & c_\eta c_\phi \end{bmatrix}$$

In Eqn. (2), $\mathbf{E}$ represents the product of XY Euler rotation angles about the axis A and it comprises of the tilt angles η and ϕ. The spring mounting points of the mobile end-effector are represented by $D_i (i = 1, 2, 3)$ with their coordinate frame given by $\sum_2$. Similar to the intermediate mobile platform, the vector coordinates can be estimated using the XY Euler angles about the axis G of the universal joint. However, this can only provide the relation between the two mobile platforms in the local frame. With reference to the fixed base, the vector coordinates of the end-effector spring mounting points are given by:

$$\mathbf{d}_{i+1} = \mathbf{e} + \mathbf{F}\, \mathbf{c}_{i+1}, \quad i = 0, 1, 2 \qquad (3)$$

$$\text{where } \mathbf{F} = \begin{bmatrix} c_\psi & 0 & s_\psi \\ s_\zeta s_\psi & c_\zeta & -s_\zeta c_\psi \\ -c_\zeta s_\psi & s_\zeta & c_\zeta c_\psi \end{bmatrix} \text{ and } \mathbf{e} = \mathbf{E} \left[0, 0, 2hr_f\right]^T$$

In Eqn. (3), $\mathbf{F}$ represents the product of XY Euler rotation angles about the axis G and it comprises of the tilt angles ζ and ψ. The vector $\mathbf{e}$ is used to create the link between the fixed base and the end-effector of the tensegrity mechanism. The Inverse Kinematics Problem (IKP) is simpler to resolve for the architecture. It involves calculating the distance between the base and the intermediate platform and the distance between the intermediate platform and the end-effector. The sum of each distance provides the solution to the IKP from the base to the mobile end-effector. The equations are given as follows:

$$l_i = \sqrt{(b_{ix} - c_{ix})^2 + (b_{iy} - c_{iy})^2 + (b_{iz} - c_{iz})^2} \qquad (4)$$

$$l_{i+3} = \sqrt{(d_{ix} - c_{ix})^2 + (d_{iy} - c_{iy})^2 + (d_{iz} - c_{iz})^2} \qquad (5)$$

$$L_i = l_i + l_{i+3} \qquad (6)$$

$$\text{with } i = 1, 2, 3 \text{ in } (4), (5) \,\&\, (6)$$

Eqn. (4) gives the IKP solution between the base and the intermediate mobile platform and Eqn. (5) gives the solutions between the intermediate mobile platform and the end-effector. The solutions to the IKP from the base to the mobile end-effector are given by Eqn. (6). Lengths l_1 to l_3 represent the spring length between the spring mounting points of the fixed base and the intermediate mobile platform. Lengths l_4 to l_6 are the spring lengths between the intermediate mobile platform and the end-effector. For given input tilt angles, the IKP can be solved using Eqns. (4) to Eqns. (6) in the Euler space.

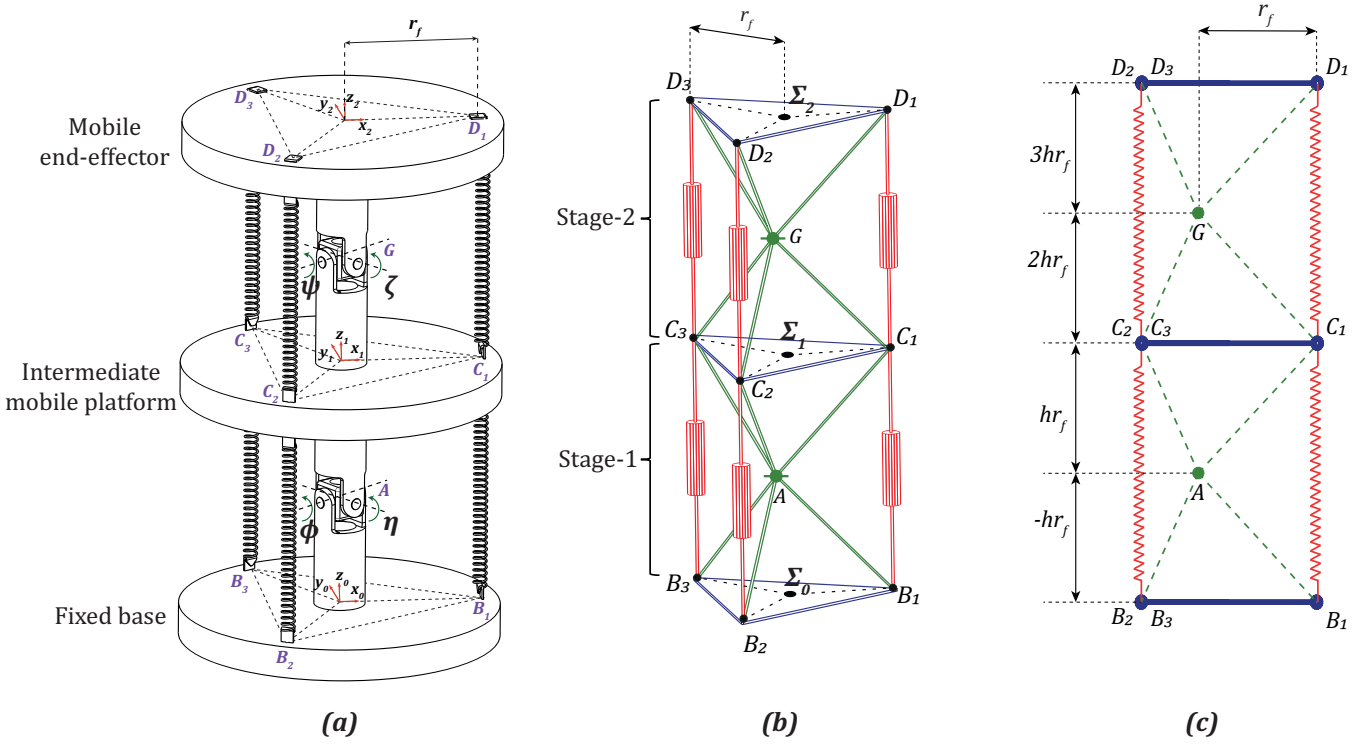

FIGURE 1: (A) THE ARCHITECTURE OF THE HYBRID TENSEGRITY MECHANISM, (B) THE CORRELATION OF THE MECHANISM TO A SERIES-PARALLEL 3-SPS-U ARCHITECTURE, (C) THE 2D VIEW OF THE HYBRID MECHANISM

2.2 Geometrical equations in the Tilt & Torsion space

The singularity analysis of the single module tensegrity mechanism was carried out using the Euler angles η and ϕ in [12]. The analysis involves considering both tilt angles in the algebraic computation and this will become complex for the architecture proposed in this article when four tilt angles are taken into account. It must also be noted that we have an architecture which has a correlation to spherical joints and there exists no torsion on the universal joint. Thus, it is possible to analyze the hybrid mechanism using the Tilt & Torsion angles presented by Bonev et al.[13]. For the single-stage mechanism, under the active modes cables were used to actuate the mobile platform. The main focus of introducing the stacked model is to have higher tilt angles when compared to the former architecture. Thus, the actuation strategy will be performed in such a way that the mobile end-effector is controlled directly through cables that pass from the three motors near the fixed base. As there exists no torsion about the universal joint, the tilt and azimuth angles will be sufficient to analyze the architecture. The representation of the tilt and azimuth angles on the hybrid mechanism is shown in Fig. 2. In Fig. 2, β represents the azimuth angle between the x_1 axis and the face of the z_1 axis for stage-1. As the actuation strategy involves controlling the mobile end-effector from the base, the azimuth angle remains the same, which is given by β between the x_2 axis and the face of the z_2 axis for stage-2. A rotation about M leads to a shift of axis from $x_1y_1z_1$ to $x_1^*y_1^*z_1^*$ for stage-1. Here the angles between z_1 and z_1^* represent the tilt angle α. Similarly, for the second stage, a rotation about N leads to a shift of axis from $x_2y_2z_2$ to $x_2^*y_2^*z_2^*$ and this provides the tilt angle δ between

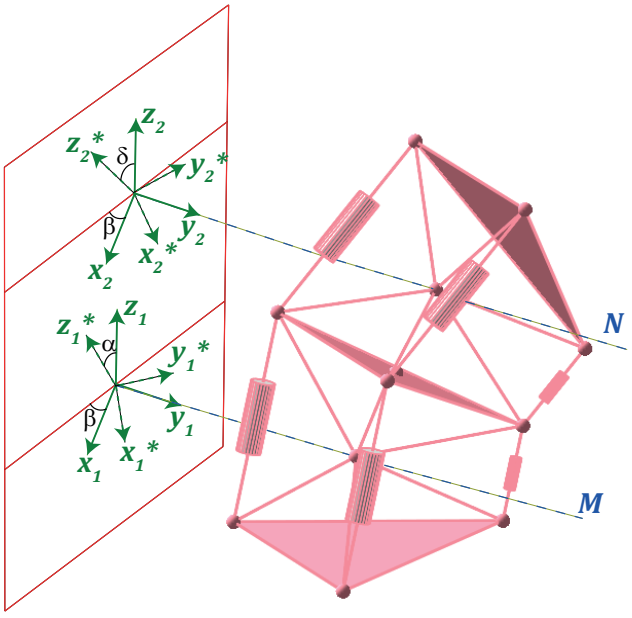

FIGURE 2: REPRESENTATION OF THE TILT AND AZIMUTH ANGLES ON THE TENSEGRITY MECHANISM

z_2 and z_2^*. The resultant transformation matrix in the T&T space for the tensegrity mechanism is thus given by the equation:

$$\mathbf{R_i} = \mathbf{R}_z(\beta)\mathbf{R}_x(X_i)\mathbf{R}_z(-\beta)\ i = 1, 2 \tag{7}$$

$$\text{where } \mathbf{R} = \begin{bmatrix} (c_{X_i} + c_\beta^2(1 - c_{X_i}) & -c_\beta s_\beta (c_{X_i} - 1) & s_\beta s_{X_i} \\ -c_\beta s_\beta (c_{X_i} - 1) & 1 + (c_{X_i} - 1)c_\beta^2 & -c_\beta s_{X_i} \\ -s_\beta s_{X_i} & c_\beta s_{X_i} & c_{X_i} \end{bmatrix}$$

$$\text{for } i = 1\ ,\ X_1 = \alpha\ \ \&\ \ \text{for } i = 2\ ,\ X_2 = \delta$$

The vector coordinates for the fixed base remains which is given in Eqn.(1). The vector coordinates of the intermediate platform and the end-effector in the T&T space are given by:

$$\mathbf{c}_{i+1} = \mathbf{R}_1 \left[r_f \cos\left(\frac{2\pi i}{3}\right), r_f \sin\left(\frac{2\pi i}{3}\right), r_f h \right]^T,\ \ i = 0, 1, 2 \quad (8)$$

$$\mathbf{d}_{i+1} = \mathbf{R}_1 \left[0, 0, 2hr_f\right]^T + \mathbf{R}_2 \mathbf{c}_{i+1},\ \ i = 0, 1, 2 \quad (9)$$

The solutions to the IKP can then be estimated by calculating the distance between the spring mounting points and these equations are given by:

$$\begin{aligned} l_{3i+1} = &-2\, rf^2 (2\ \sin(\beta) \sin(X_i)\, h - (\cos(\beta))^2 \cos(X_i) - \\ &\cos(X_i)\, h^2 + (\cos(\beta))^2 - h^2 + \cos(X_i) - 1) \end{aligned} \quad (10)$$

$$\begin{aligned} l_{3i+2} = &\ 0.5\, rf^2 (-2\ \sin(\beta) \cos(\beta) \cos(X_i)\ \sqrt{3} + 4\, h^2 - \cos(X_i) \\ &+ 4\ \sqrt{3} \cos(\beta) \sin(X_i)\, h + 4\ \sin(\beta) \sin(X_i)\, h + 2\ (\cos(\beta))^2 \\ &+ 2\ \cos(\beta)\ \sqrt{3} \sin(\beta) - 2\ (\cos(\beta))^2 \cos(X_i) \\ &+ 4\ \cos(X_i)\, h^2 + 1) \end{aligned} \quad (11)$$

$$\begin{aligned} l_{3i+3} = &\ 0.5\, rf^2 (2\ \sin(\beta) \cos(\beta) \cos(X_i)\ \sqrt{3} + 4\, h^2 - \cos(X_i) \\ &- 4\ \sqrt{3} \cos(\beta) \sin(X_i)\, h + 4\ \sin(\beta) \sin(X_i)\, h + 2\ (\cos(\beta))^2 \\ &- 2\ \cos(\beta)\ \sqrt{3} \sin(\beta) - 2\ (\cos(\beta))^2 \cos(X_i) \\ &+ 4\ \cos(X_i)\, h^2 + 1) \end{aligned} \quad (12)$$

$$\text{where } i\ = 0, 1\ \&\ \text{for } i = 0\ ,\ X_0 = \alpha\ \ \&\ \ \text{for } i = 1\ ,\ X_2 = \delta$$

In the T&T space, the mechanism can be analyzed using two tilt angles and a common azimuth for the entire assembly under the assumption that there exists no friction between each module and the connecting elements. The T&T space will thus be employed for further analysis of the mechanism.

3. STABILITY ANALYSIS OF THE MECHANISM

Based on the analysis presented in [11], we have incorporated the inverse pendulum configuration stacked one over the other. By nature, this configuration is unstable even in the absence of applied forces. In this section, the stability analysis of the mechanism is carried out by an optimization approach to determine the design parameters of the mechanism. According to Lagrange, the equation of motion for a moving system is given by [17]:

$$\boldsymbol{\tau} = \frac{\mathrm{d}}{\mathrm{d}t}\left(\frac{\partial T}{\partial \dot{\mathbf{q}}}\right) - \frac{\partial T}{\partial \mathbf{q}} + \frac{\partial U}{\partial \mathbf{q}} \ \text{ where } \ \mathbf{q} = [\alpha, \delta, \beta]^T \quad (13)$$

In Eqn. (13), T and U represents the kinetic and potential energies of the system. $\boldsymbol{\tau}$ represents the generalized torques on the system. As the stability analysis is carried out in the static mode, the kinetic energy terms becomes zero in Eqn. (13). The potential energy of the system is contributed by the tension springs and the cables that control each platform. For this analysis, we consider the magnitude of applied forces as F_1 to F_6 along each cable and an identical tension spring of stiffness k N/mm. Thus, the potential energy equations for the system are given by:

$$U_{cable} = \sum_{i=1}^{6} F_i l_i \quad U_{spring} = \sum_{i=1}^{6} \frac{1}{2} k l_i^2 \quad (14)$$

$$U_{tot} = U_{cable} + U_{spring} \quad (15)$$

We consider the springs to be massless and their zero free lenghts are set to zero. The spring lengths l_1 to l_6 can be computed using the Eqns. (10) to (12) for input tilt and azimuth angles.

3.1 Optimum design parameters

As we have a stacked model, it is essential to ensure that the mechanism remains stable in the home-pose condition and the presence of a pre-load. As the mechanism is proposed to be integrated with the piping inspection robot studied in [10], the value of r_f is taken as 11 mm, which is in line with the flange dimensions of the piping inspection robot. We assume a pre-loading of 2 N along each i.e., F_1 to $F_6 = 2$ N. The tilt and azimuth work in such a way that the mechanism is initially tilted along one of the directions. Once the desired tilt is reached, the tilt angle remains constant and the azimuth completes a revolution from 0 to 2π radians or vice-versa. During the tilt stage, the azimuth does not influence the stability and we analyze the stability during the tilt phases. The total potential energy is calculated under these conditions and an equation is obtained which is a function of the tilt angles α, δ, the design parameter h and the spring stiffness k. It is represented by:

$$U_{tot} = f(\alpha, \delta, k, h)) \text{ at } \beta = 0 \text{ radian} \quad (16)$$

From Eqn. (16), we can observe that the total potential energy of the system has dependencies on the two tilt angles. For analyzing the static stability, it is necessary to study the Hessian matrix, also known as the mechanism stiffness. The determinant of this matrix and the second-order derivative of the total potential energy with respect to one of the tilt angles are then calculated. The Hessian matrix and its determinant are given by:

$$\mathbf{H} = \begin{bmatrix} \frac{\partial^2 U_{tot}}{\partial \alpha^2} & \frac{\partial^2 U_{tot}}{\partial \alpha \partial \delta} \\ \frac{\partial^2 U_{tot}}{\partial \alpha \partial \delta} & \frac{\partial^2 U_{tot}}{\partial \delta^2} \end{bmatrix} = \begin{bmatrix} f_{11} & f_{12} \\ f_{21} & f_{22} \end{bmatrix} \quad (17)$$

$$\det(\mathbf{H}) = f_{11} f_{22} - f_{12}^2 \quad (18)$$

For ensuring the stability of the architecture, the total potential energy must be a relative minimum which occurs when $\det(\mathbf{H}) > 0$ and $f_{11} > 0$. An optimization problem is solved

at the home-pose condition where the tilt angles are zero. This problem will help in identifying the remaining design parameters h and k. Generally, optimization problems can be classified into Deterministic and Heuristic approaches [18]. A deterministic approach using the function $fmincon$ is carried out in MATLAB. The optimization problem is stated as:

$$\text{Maximize: } f_{11}(\mathbf{x})$$

$$\text{subject to constraints: } g_1\text{: } \det(\mathbf{H}) \geq 0 \ , \ g_2\text{: } f_{11}(\mathbf{x}) \geq 0$$

$$\text{where } \mathbf{x} = [h, k]^T \text{ , lb} = [0.5, 0.5] \ \ \& \ \ \text{ub} = [1, 4]$$

The objective function aims to maximize the second-order derivative of the total potential energy for one of the tilt angles and we consider f_{11}. The inequality constraints g_1 and g_2 ensure that the determinant of the Hessian given matrix and the objective function remains positive throughout the optimization algorithm. The lower bounds for h and k are set as 0.5 and 0.5 whereas the upper bounds are set as 1 and 4. For h, the value cannot exceed 1 based on the earlier findings [10]. The equations of the determinant value and the second-order derivative at the home-pose are given by:

$$\det(\mathbf{H}) = \frac{1089}{4}\left(22\,h^2k + 2h^2 - 11\,k\right)^2 \tag{19}$$

$$f_{11} = -363\,h^2k + \frac{363}{2}\,k - 33h^2 \tag{20}$$

With the optimization problem being defined, the deterministic approach was carried out in MATLAB. From the results of optimization, the values were found to be h= 0.6761 and k= 2 N/mm. These are the optimum or the maximum values of h and k that ensure the static stability of the mechanism in the home-pose. For ensuring safer operations and rounding the stiffness to the standard size, the values are set at h= 0.6 and k= 2 N/mm. The total potential energy of the system is estimated for these design parameters at the home-pose and the plot is represented in Fig. 3. From Fig. 3, we can observe a relative minimum of the total potential energy around the home-pose, thereby ensuring the static stability of the mechanism. Thus, the design parameters h= 0.6 and k = 2 N/mm will be retained for further analysis of the architecture.

4. ANALYSIS OF WORKSPACE FOR THE HYBRID MECHANISM

With the optimum design parameters being determined through stability analysis, the next step is to determine the feasible workspace of the tensegrity mechanism. This is carried out by the singularity analysis of the architecture and this analysis is important to determine the maximum tilt limits. Similar to the single-stage model, the singularity analysis for the stacked tensegrity mechanism is carried out using the well-known velocity model [19]:

$$\mathbf{At} + \mathbf{B}\dot{\rho} = 0 \tag{21}$$

where $\mathbf{t}$ represents the angular velocity vector

and $\dot{\rho} = [\dot{l_1}, \dot{l_2}, \dot{l_3}, \dot{l_4}, \dot{l_5}, \dot{l_6}]^T$ represents the joint velocity vector

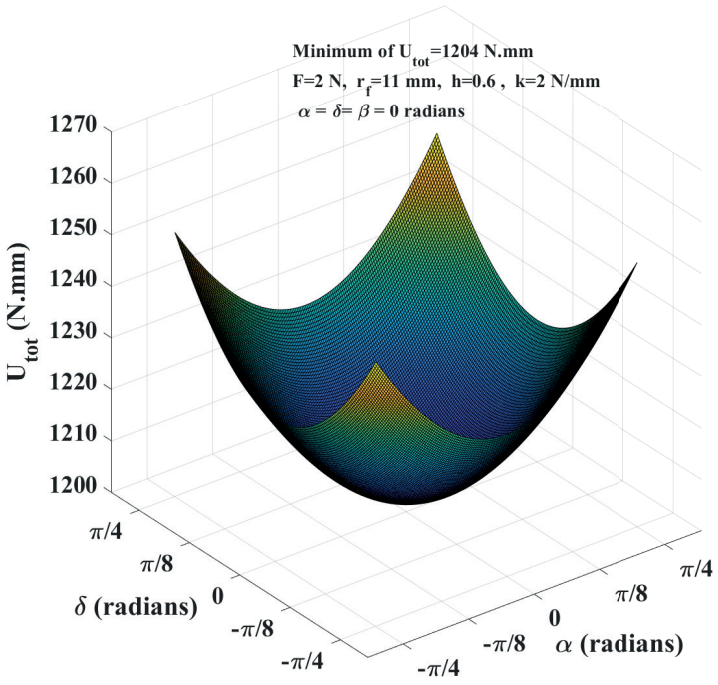

FIGURE 3: PLOT OF THE TOTAL POTENTIAL ENERGY OF THE SYSTEM AT THE HOME-POSE AT h=0.6 AND k=2 N/MM

In Eqn. (21), **A** represents the direct-kinematics matrix or forward Jacobian matrix and **B** represents the inverse-kinematics matrix or inverse Jacobian matrix. The singularity analysis will be carried out in the T&T space wherein the pose variables are given by the angles α, β and δ. The articular variables are the spring lengths l_1 to l_6. It has to be noted that the spring lengths represented here are estimated by solving the IKP in the T&T space.

For the hybrid mechanism under study, it can have three types of singularities namely: Type-1, Type-2 and Type-3 [20]. The Type-1 or serial singularities can occur when the determinant of the matrix **B** becomes zero. This scenario occurs only when the length of one of the six prismatic springs becomes zero, which is not possible for the mechanism. Thus, there exist no serial singularities for the mechanism. Type-2 singularities occur when the determinant of the matrix **A** becomes zero and this will be verified by differentiating the solutions of the IKP with respect to the pose variables. The Type-3 singularities occur only when there exist both serial and parallel singularities, which is once again not possible for the mechanism. Based on the experiments conducted on the tensegrity mechanism in [21], it was observed that one or two of the prismatic springs reach their minimum length at two specific positions referred to as:

- One spring pull: One of the spring pulls while the other two springs pushes the mobile platform
- Two springs pull: Two of the springs pulls while the third spring pushes the mobile platform

Also, these are the two positions where the mechanism reaches the maximum tilt. Along the side B_1, C_1, D_1, the one spring

pull and two springs pull can be observed at azimuth angles of β= 0 radian and β=π radians. Thus, the singularity analysis can be simplified by identifying the maximum tilt angles α and δ at these azimuth positions. The other positions of the one spring and two springs pull can be observed at a phase difference of $2\pi/3$ radians. However, it is sufficient to analyze along one side as the same results will be obtained along each side. It must be noted that this simplification cannot be done if the mechanism is analyzed in the Euler space as for each position of the mechanism, all four tilt angles must be taken into account.

4.1 Singularity analysis using the CAD algorithm

With fixed values for the azimuth angle β, the hybrid mechanism now has two pose variables α, δ and six articular variables (l_1 to l_6). Based on these number of variables, we can observe that the direct kinematics matrix $\mathbf{A}$ does not correspond to a $n \times n$ square matrix. Thus, we split the architecture into three sets of hybrid 1-SPS-U architectures which comprise of length pairs $l_1 - l_4$, $l_2 - l_5$ and $l_3 - l_6$. The matrices are given by:

$$\mathbf{A}_{i-i+3} = \begin{bmatrix} \frac{\partial l_i}{\partial \alpha} & \frac{\partial l_i}{\partial \delta} \\ \frac{\partial l_{i+3}}{\partial \alpha} & \frac{\partial l_{i+3}}{\partial \delta} \end{bmatrix}, i = 1, 2, 3 \tag{22}$$

In Eqn. (22), l_i represents the length of the i^{th} prismatic spring which can be computed using the IKP Eqns. (10) to (12). The direct kinematics matrix is then constructed for each length pairs. The determinant equations are represented by $\mathfrak{D}_{p1}$, $\mathfrak{D}_{p2}$ and $\mathfrak{D}_{p3}$ for the length pairs $l_1 - l_4$, $l_2 - l_5$ and $l_3 - l_6$ respectively. Since the one spring and two springs pull configurations are considered for analysis, two of the determinant equations appear similar. For β at 0 and π radians, values of $\mathfrak{D}_{p2}$ and $\mathfrak{D}_{p3}$ are identical. The determinant equations are given by:

$$\begin{aligned} \mathfrak{D}_{p1} : (&\sin(\alpha)\, h^4 \sin(\delta) + 2\, \sin(\alpha)\, h^3 \cos(\delta) + \sin(\delta) \sin(\alpha) \\ &2m\, \sin(\alpha)\, h^2 \sin(\delta) + 2m\, \cos(\alpha)\, h^3 \sin(\delta) - \\ &- 2m\, \sin(\delta) \cos(\alpha)\, h - 2m\, \sin(\alpha) \cos(\delta)\, h + \\ &4\, \cos(\alpha)\, h^2 \cos(\delta)) = 0 \end{aligned} \tag{23}$$

$$\begin{aligned} \mathfrak{D}_{p2} = \mathfrak{D}_{p3} : (&16\, \sin(\alpha)\, h^4 \sin(\delta) - 16m\, \sin(\alpha)\, h^3 \cos(\delta) \\ &- 8\, \sin(\alpha)\, h^2 \sin(\delta) - 16m\, \cos(\alpha)\, h^3 \sin(\delta) \\ &+ 16\, \cos(\alpha)\, h^2 \cos(\delta) + 4m\, \sin(\delta) \cos(\alpha)\, h \\ &+ 4m\, \sin(\alpha) \cos(\delta)\, h + \sin(\delta) \sin(\alpha)) = 0 \end{aligned} \tag{24}$$

where $m = 1$ at $\beta = 0$ & $m = -1$ at $\beta = \pi$ in (23) & (24)

For identifying the feasible workspaces of the architecture, the SIROPA library of Maple is employed [22]. This library is an efficient tool which is employed for the analysis of parallel robots and their singular configurations [23]. Using the $CreateManipulator$ function of SIROPA, the hybrid parallel mechanism is constructed in Maple using the geometric equations and IKP equations in the T&T space. For the singularity analysis, we also set joint limits for each spring and they are set as l_{min} = 7 mm and l_{max} = 31 mm. The IKP equations of each spring are set at these limits and a total of 12 equations (2 for each spring for each limit) are generated using the $ConstraintEquations$ function of SIROPA. The joint limits are essential to identify the singularity boundaries for the mechanism and extract the feasible workspace. Eqns. (23) to (24) are generated using the $ParallelSingularities$ function of SIROPA and the values of h and k are set at 0.6 and 2 N/mm from the results of the optimization problem. The singularity analysis is then carried out using the modified Cylindrical Algebraic Decomposition (CAD) algorithm in Maple. In the SIROPA library, the modified CAD algorithm is employed along with the Groebner base elimination technique. The Groebner base elimination technique is useful for the computation of a subset of the workspace where the number of solutions changes and this is referred to as the Discriminant Variety. In Maple, this is possible using the $RootFinding[Parametric]$ function. The function $CellDecompositionPlus$ of SIROPA library combines the CAD algorithm with the root finding parametric technique and this function is used to identify solutions to the Direct Kinematic Problems (DKP). For isolating the aspects around the home-pose, the IKP equations are transformed into inequality equations for the $CellDecompositionPlus$ function [24].

4.2 Results of the singularity analysis

The CAD algorithm was executed for each azimuth angle considered for the analysis. The results of the feasible workspace obtained by the CAD algorithm are summarized below:

1. The first analysis was carried out at β= 0 radians. The results obtained from this analysis is shown in Fig. 4a. The magenta zone represents the cells where there exists one solution to the DKP. The grey region indicate the zone where there exists no solutions to the DKP. Around the home-pose, the mechanism has tilt limits bounded by $\mathbf{S} : [s_1, s_2] \in [-\pi/3, \pi/6]$ radians. Here s_1 and s_2 refers to the minimum and maximum extemities of the tilt angles α and δ. Beyond the gray zones, there also exists some cells with solutions to the DKP however these regions are not accessible for the mechanism as it can lead to the architecture being locked in singular configurations.

2. Followed by that, the second analysis was carried out with $\beta = \pi$ radians and the results are represented in Fig. 4b. The cyan region indicates the cells where there exists one solution to the DKP whereas the grey region represent no solutions. For this azimuth configuration, the minimum and maximum extremities of the tilt angles around the home-pose are bounded by $\mathbf{T} : [t_1, t_2] \in [-\pi/6, \pi/3]$ radians.

3. When a circular trajectory is performed using the mechanism, the azimuth angle can vary from 0 to 2π radians. During this trajectory, the one-spring and two-spring pull configurations could be observed for the mechanism. The overall tilt limits for the mechanism can thus be obtained by merging the solutions obtained from each analysis. The solution obtained by merging the results of each analysis from CAD is shown in Fig. 4c. The orange region represents the singularity-free workspace of the hybrid mechanism. The

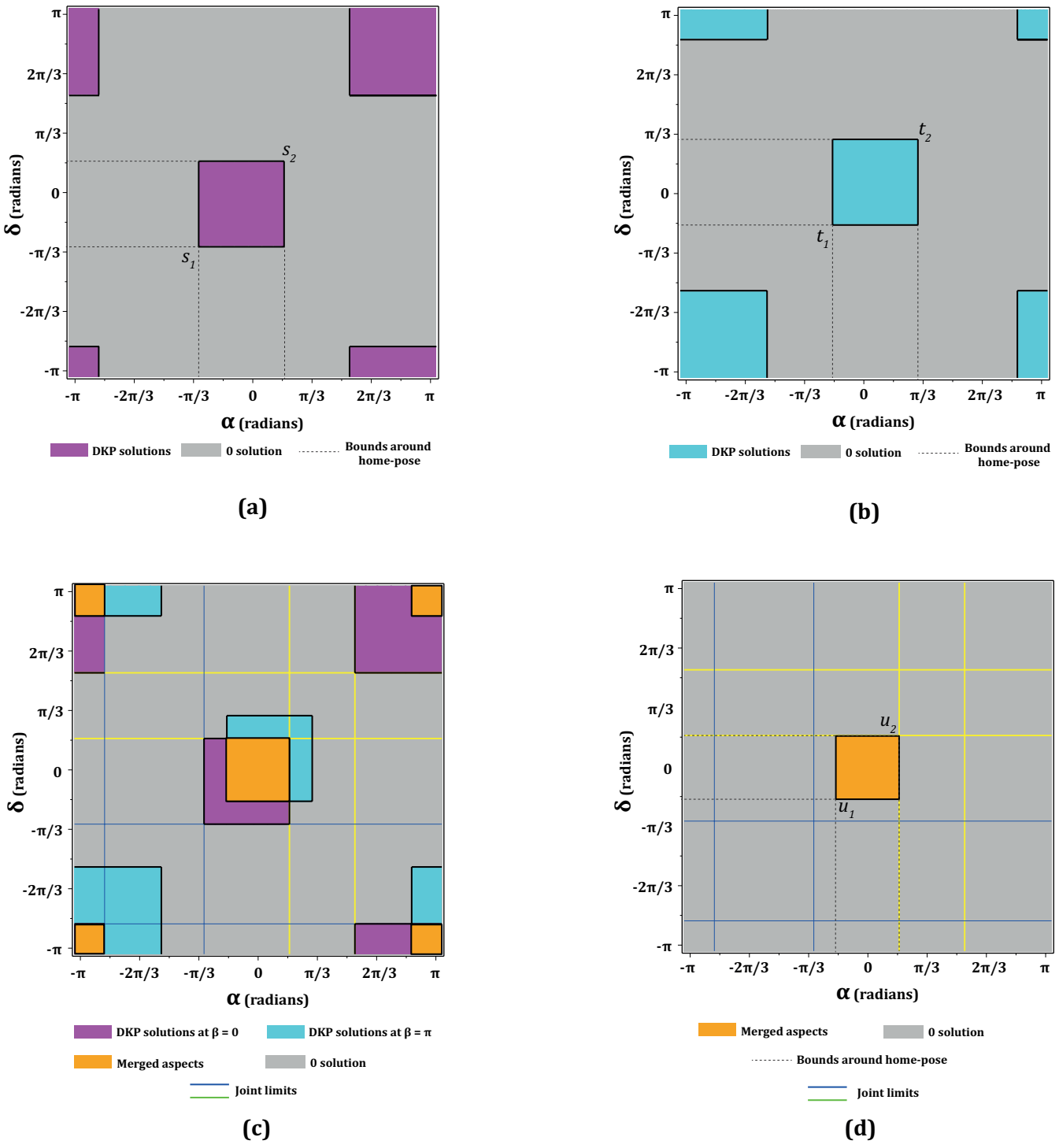

FIGURE 4: RESULTS OBTAINED BY CAD ALGORITHM IN MAPLE WITH THE REPRESENTATION OF FEASIBLE AND NON-FEASIBLE SOLUTIONS: (A) AT β = 0 RADIANS (B) AT $\beta = \pi$ RADIANS, (C) BY MERGING THE TWO INITIAL SOLUTIONS AND (D) BY ISOLATING THE ASPECTS AROUND THE HOME-POSE FOR THE MECHANISM ALONG WITH THE JOINT LIMITS FOR EACH SPRING SET AT l_{min} = 7 MM AND l_{max} = 31 MM

solutions to the IKP with the joint limits are also represented by the blue and yellow lines for each prismatic spring.

4. In Fig. 4d, only the feasible solutions around the home-pose are isolated. The singularity-free workspace for the hybrid mechanism is thus defined by:

$$\mathbf{S} \cap \mathbf{T} \longrightarrow \mathbf{U} : [u_1, u_2] \in [-\pi/6, \pi/6] \text{ radians}$$

Based on the findings, we can conclude that the limits for each

tilt angle are given by: $\alpha = \delta = [-\pi/6, \pi/6]$ radians. Thus, the overall tilt limits for the stacked module are bounded by $\pm\pi/3$ radians.

5. MAPPING THE T&T SPACE TO EULER SPACE AND ACTUATION STRATEGY

The CAD algorithm helped in identifying the tilt limits of the mechanism. However, this was carried out in the T&T space. The results obtained from the earlier analysis must be mapped for the Euler angles of the universal joint. For performing a circular trajectory in the Euler space, the mechanism is initially tilted along one of the springs and then the circular path is initiated. The governing relationships between the T&T space and the Euler space are provided below in Table 1. As mentioned in the previous sections, the actuation strategy is proposed to be carried out by actuating the mobile end-effector through three DC-motors near the fixed base. The corresponding relations for this actuation strategy is provided in Table 1. It could be observed that once the tilt is performed, the tilt angles in the Euler space are computed as a function of the tilt and azimuth angles from the T&T space. For the stage-1, the tilt angles η and ϕ are computed with respect to α and β whereas for stage-2, the tilt angles ζ and ϕ are computed as functions of δ and β. Once the circular path is completed, the mechanism is tilted back to its home-pose. The simulation of the hybrid 3-SPS-U tensegrity mechanism can be found in the link provided at the bottom of this page [1]. From the numerical simulations, we can observe the mapping relation between both spaces. The corresponding solutions to the IKP could also be observed at each position in the simulation and they are calculated as a function of the tilt angles of their respective spaces. It has to be noted that a common azimuth for the entire assembly assuming that there exists no friction between each module and the connecting elements. The experimental setup will then be validated in the future and the actuation strategy will follow a similar approach that was presented in [21]. An overview of the experimental platform developed at LS2N, France is shown in Fig. 5.

6. CONCLUSION

A series-parallel hybrid tensegrity mechanism was presented and analyzed in this article. By correlating to a parallel manipulator of type 3-SPS-U, the geometrical equations and the vector coordinates of each platform were estimated. The Euler angles of the universal joint helped in positioning the mobile platforms and also in solving the IKP. Since the Euler space necessitates taking into account all four tilt angles of the mechanism, the theory of T&T was employed to analyze the mechanism. The T&T angles reduced the complexity in analyzing the mechanism as a common azimuth was sufficient for each stage under the assumption that there was no friction between each module. The stability analysis was then carried out which helped in identifying the design parameters h and spring stiffness k. By taking into account the Hessian matrix, an optimization approach was followed in MATLAB to ensure the static stability of the mechanism at the home-pose. The singularity analysis was carried out in two steps which involved fixing the azimuth angles at positions where one or two prismatic springs reach their minimum length. With the help of SIROPA library in Maple, the parallel singularities for the mechanism were analyzed for the two azimuth positions using the CAD algorithm. By merging the solutions obtained for each azimuth position, it was found that the maximum tilt limit for each stage was around $\pm\pi/6$ radians, thus leading to an overall tilt limit of $\pm\pi/3$ radians for the mechanism. The relationship between the T&T space and the Euler space was demonstrated to validate the results of singularity analysis. A simulation was also performed to demonstrate the relationship between these two spaces.

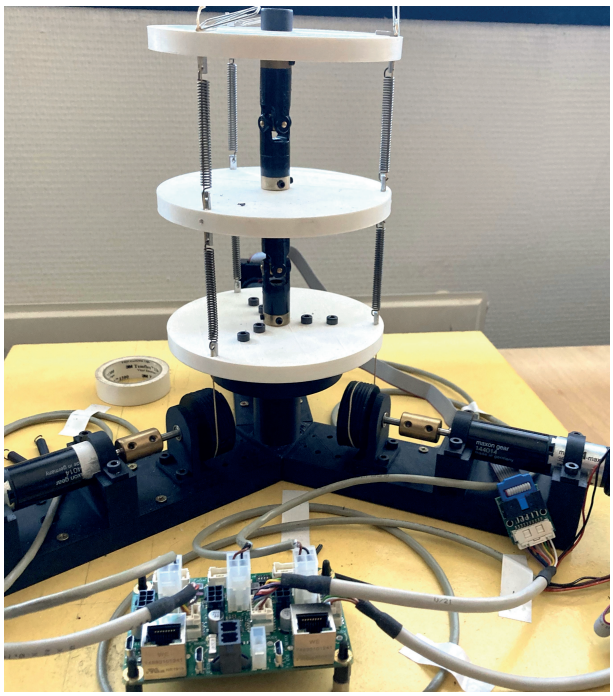

FIGURE 5: THE EXPERIMENTAL SETUP FOR THE CONTROL OF THE HYBRID 3-SPS-U TENSEGRITY MECHANISM

Currently, experiments on the hybrid mechanism are being carried out. An overview of the experimental setup was also demonstrated. The simulation that was presented in this article will be validated using the experimental platform. However, the frictional forces will come into play due to the presence of connecting elements between each module. Thus, a control law will be implemented which takes into account the friction and cable elasticity factors similar to the control strategy of a tensegrity structure proposed by Fasquelle et al.[25]. Also, advanced controllers such as the EtherCAT will be employed for the experiments when compared to a simple BeagleBone black card that was employed for the single-stage model in [21]. The EtherCAT allows controlling several components at the same time from a central unit. As the hybrid mechanism is proposed to be integrated with the inspection robot presented in [10], the EtherCAT can be useful in controlling each module of the robot assembly from a central unit.

[1] Simulation of the mechanism in MATLAB (full screen recommended): 1x Speed, 0.4x Speed

TABLE 1: MAPPING RELATION BETWEEN THE T&T SPACE AND THE EULER SPACE

Movement type	Tilt space			Euler space			
	α **(radians)**	δ **(radians)**	β **(radians)**	η **(radians)**	ϕ **(radians)**	ζ **(radians)**	ψ **(radians)**
Initial tilt	$0 \rightarrow \pi/6$	$\rightarrow \pi/6$	0	0	$0 \rightarrow \pi/6$	0	$0 \rightarrow \pi/6$
Circular path	$\pi/6$	$\pi/6$	$0 \rightarrow 2\pi$	$\alpha \sin(\beta)$	$\alpha \cos(\beta)$	$\delta \sin(\beta)$	$\delta \cos(\beta)$
Return to home	$\pi/6 \rightarrow 0$	$\pi/6 \rightarrow 0$	0	0	$\pi/6 \rightarrow 0$	0	$\pi/6 \rightarrow 0$

NOMENCLATURE

PKM	Parallel Kinematic Machines
T&T	Tilt & Torsion
CAD	Cylindrical Algebraic Decomposition
IKP	Inverse Kinematic Problem
DKP	Direct Kinematic Problem
$\mathbf{b}_i$	Vector coordinates for base B_i
$\mathbf{c}_i$	Vector coordinates of intermediate mobile platform C_i
$\mathbf{d}_i$	Vector coordinates of end-effector D_i
r_f	Distance of spring mounting point in mm
k	Stiffness of springs in N/mm
h	Design constant of the mechanism (no unit)
$\mathbf{E}$	Euler angle transformation matrix for stage-1
$\mathbf{F}$	Euler angle transformation matrix for stage-2
η, ϕ	Euler rotation angles of stage-1
ζ, ψ	Euler rotation angles of stage-2
l_i	Length of i^{th} prismatic spring
$\mathbf{R}_1$	Tilt & Azimuth transformation matrix for stage-1
$\mathbf{R}_2$	Tilt & Azimuth transformation matrix for stage-1
α	Tilt angle of stage-1 in T&T space
δ	Tilt angle of stage-2 in T&T space
β	Azimuth angle of the mechanism
F_i	Magnitude of the applied force along the i^{th} cable
$\mathbf{H}$	Hessian matrix
$\mathbf{A}$	Direct kinematics matrix
$\mathbf{B}$	Inverse kinematics matrix
$\mathcal{D}$	Determinant value of the direct kinematics matrix

REFERENCES

[1] Merlet, Jean-Pierre. "Parallel robots: Open problems." *Robotics Research: The Ninth International Symposium*: pp. 27–32. 2000. Springer.

[2] Tsai, Lung-Wen. *Robot analysis: the mechanics of serial and parallel manipulators*. John Wiley & Sons (1999).

[3] Miller, Karol. "Optimal design and modeling of spatial parallel manipulators." *The International Journal of Robotics Research* Vol. 23 No. 2 (2004): pp. 127–140.

[4] Carbone, Giuseppe and Ceccarelli, Marco. "A stiffness analysis for a hybrid parallel-serial manipulator." *Robotica* Vol. 22 No. 5 (2004): pp. 567–576.

[5] Yeshmukhametov, Azamat, Kalimoldayev, Maksat, Mamyrbayev, Orken and Amirgaliev, Yedilhan. "Design and kinematics of serial/parallel hybrid robot." *2017 3rd International Conference on Control, Automation and Robotics (ICCAR)*: pp. 162–165. 2017. IEEE.

[6] Eβer, Julian, Kumar, Shivesh, Peters, Heiner, Bargsten, Vinzenz, de Gea Fernandez, Jose, Mastalli, Carlos, Stasse, Olivier and Kirchner, Frank. "Design, analysis and control of the series-parallel hybrid RH5 humanoid robot." *2020 IEEE-RAS 20th International Conference on Humanoid Robots (Humanoids)*: pp. 400–407. 2021. IEEE.

[7] Sun, Huihui, Zhang, Yujie, Xie, Bin and Zi, Bin. "Dynamic modeling and error analysis of a cable-linkage serial-parallel palletizing robot." *IEEE Access* Vol. 9 (2020): pp. 2188–2200.

[8] Huang, Qitao, Wang, Peng, Wang, Yuhao, Xia, Xiaohua and Li, Songjing. "Kinematic Analysis of Bionic Elephant Trunk Robot Based on Flexible Series-Parallel Structure." *Biomimetics* Vol. 7 No. 4 (2022): p. 228.

[9] Nayak, Abhilash, Caro, Stéphane and Wenger, Philippe. "Kinematic analysis of the 3-RPS-3-SPR series–parallel manipulator." *Robotica* Vol. 37 No. 7 (2019): pp. 1240–1266.

[10] Venkateswaran, Swaminath, Chablat, Damien and Boyer, Frédéric. "Numerical and experimental validation of the prototype of a bio-inspired piping inspection robot." *Robotics* Vol. 8 No. 2 (2019): p. 32.

[11] Venkateswaran, Swaminath, Furet, Matthieu, Chablat, Damien and Wenger, Philippe. "Design and analysis of a tensegrity mechanism for a bio-inspired robot." *International Design Engineering Technical Conferences and Computers and Information in Engineering Conference*, Vol. 59230: p. V05AT07A026. 2019. American Society of Mechanical Engineers.

[12] Venkateswaran, Swaminath and Chablat, Damien. "Singularity and Workspace Analysis of 3-SP SU and 4-SP SU Tensegrity Mechanisms." *Advances in Robot Kinematics 2020*: pp. 226–233. 2021. Springer.

[13] Bonev, IA, Zlatanov, D and Gosselin, Clément M. "Advantages of the modified Euler angles in the design and control of PKMs." *2002 Parallel Kinematic Machines International Conference*: pp. 171–188. 2002. Citeseer.

[14] Bonev, Ilian A and Ryu, Jeha. "Orientation workspace analysis of 6-DOF parallel manipulators." *International Design Engineering Technical Conferences and Computers and Information in Engineering Conference*, Vol. 19715: pp. 281–288. 1999. American Society of Mechanical Engineers.

[15] Briot, Sébastien and Bonev, Ilian A. "Singularity analysis of zero-torsion parallel mechanisms." *2008 IEEE/RSJ international conference on intelligent robots and systems*: pp. 1952–1957. 2008. IEEE.

[16] Alici, Gürsel and Shirinzadeh, Bijan. "Topology optimisation and singularity analysis of a 3-SPS parallel manipulator with a passive constraining spherical joint." *Mechanism and Machine Theory* Vol. 39 No. 2 (2004): pp. 215–235.

[17] Meirovitch, Leonard. *Fundamentals of vibrations*. Waveland Press (2010).

[18] Guessasma, S and Bassir, HD. "Comparing heuristic and deterministic approaches to optimise mechanical parameters of biopolymer composite materials." *Mechanics of Advanced Materials and Structures* Vol. 16 No. 4 (2009): pp. 293–299.

[19] Gosselin, Clement, Angeles, Jorge et al. "Singularity analysis of closed-loop kinematic chains." *IEEE transactions on robotics and automation* Vol. 6 No. 3 (1990): pp. 281–290.

[20] Wenger, Philippe and Chablat, Damien. "Definition sets for the direct kinematics of parallel manipulators." *1997 8th International Conference on Advanced Robotics. Proceedings. ICAR'97*: pp. 859–864. 1997. IEEE.

[21] Venkateswaran, Swaminath and Chablat, Damien. "Trajectory Planning for a 3-SP SU Tensegrity Mechanism." *International Design Engineering Technical Conferences and Computers and Information in Engineering Conference*, Vol. 85451: p. V08BT08A004. 2021. American Society of Mechanical Engineers.

[22] Jha, Ranjan, Chablat, Damien, Baron, Luc, Rouillier, Fabrice and Moroz, Guillaume. "Workspace, joint space and singularities of a family of delta-like robot." *Mechanism and Machine Theory* Vol. 127 (2018): pp. 73–95.

[23] Chablat, Damien, Moroz, Guillaume, Rouillier, Fabrice and Wenger, Philippe. "Using Maple to analyse parallel robots." *Maple in Mathematics Education and Research: Third Maple Conference, MC 2019, Waterloo, Ontario, Canada, October 15–17, 2019, Proceedings 3*: pp. 50–64. 2020. Springer.

[24] Chablat, Damien and Wenger, Philippe. "Working modes and aspects in fully parallel manipulators." *Proceedings. 1998 IEEE International Conference on Robotics and Automation (Cat. No. 98CH36146)*, Vol. 3: pp. 1964–1969. 1998. IEEE.

[25] Fasquelle, Benjamin, Khanna, Parag, Chevallereau, Christine, Chablat, Damien, Creusot, Denis, Jolivet, Stéphane, Lemoine, Philippe and Wenger, Philippe. "Identification and control of a 3-X cable-driven manipulator inspired from the Bird's neck." *Journal of Mechanisms and Robotics* Vol. 14 No. 1 (2022).